Crystallographic contribution to the vital effect in biogenic carbonates Mg/Ca thermometry

Alberto Pérez-Huerta[1]*, Maggie Cusack[2] and Paul Dalbeck[2]

[1] Department of Geological Sciences, University of Alabama, Tuscaloosa AL 35487, USA
Email: aphuerta@as.ua.edu

[2] School of Geographical & Earth Sciences, University of Glasgow, G12 8QQ Glasgow, UK

*Corresponding author.

ABSTRACT: The processes involved in vital effects, defined as biological processes overriding environmental signals, are not well understood and this hampers the interpretation of environmental parameters such as seawater temperature. Insufficient knowledge is available about changes in physico-chemical parameters, in particular those related to crystallography, associated with biomineral formation and emplacement. This paper assesses the influence of crystallography on Mg^{2+} concentration and distribution in calcite biominerals of bivalved marine organisms, mussels and rhynchonelliform brachiopods, and considers the implications for Mg/Ca thermometry. In the mussel *Mytilus edulis*, changes in Mg^{2+} are not associated with crystallography; but in the brachiopod *Terebratulina retusa*, increases in Mg^{2+} concentrations ($\sim$0·5–0·6 wt. %) are associated with the {0001} planes of calcite biominerals. A comparison between mussels and brachiopods with avian eggshells, which form at constant ambient temperature, also reveals that there is at least a common 0·1 wt. % variation in magnesium concentration in these calcite biomineral systems unrelated to temperature or crystallography. Results demonstrate that the integration of contextual crystallographic, biological and chemical information may be important to extract accurate environmental information from biominerals.

KEY WORDS: Brachiopod, calcite, c-axis, magnesium, mussel, sector zoning

Vital effects are a major obstacle to the fidelity of the seawater temperature recorded in carbonate biogenic minerals, via chemical proxies such as stable isotopes and trace elements, to calcium ratios (Urey *et al.* 1951). The use of the term 'vital effect' has, however, become a 'black box' term to designate any aspect that hampers the environmental interpretation, but with the absence of a deep understanding of the processes involved (Weiner & Dove 2003). Significant advances have been made in our understanding of kinetic and taxonomic effects, as well as of the physiological processes related to these vital effects, with detailed studies in several groups of organisms such as foraminifera (e.g., Erez 2003) and corals (e.g., Cohen & McConnaughey 2003). Less knowledge is available about the influence of physico-chemical parameters associated with biomineral formation and emplacement within the context of biological control, which has a specific effect on trace elements (Mg^{2+} and Sr^{2+}) used in seawater temperature calculations. In particular, the effect on trace element distribution and concentration associated with crystallographic orientation of biominerals has been an unknown factor. This is significant, since trace element concentrations vary in crystal faces of non-biogenic carbonates related to differences in the solution–crystal partitioning ('sector zoning') (Reeder & Grams 1987; Reeder & Paquette 1989). The present paper analyses the influence of crystallography on Mg^{2+} concentration and distribution in calcite biominerals of bivalved marine organisms (mussels and rhynchonelliform brachiopods) and considers the implications for Mg/Ca thermometry. In addition, mussels and brachiopods are compared to calcitic avian eggshells which form under constant ambient temperature.

The blue mussel *Mytilus edulis* (Dalbeck *et al.* 2006; Cusack *et al.* 2007) and the rhynchonelliform brachiopod *Terebratulina retusa* (Cusack *et al.* 2007; England *et al.* 2007) have been partially characterised on an individual basis in terms of crystallographic variation and the distribution and concentration of trace elements. Integration of this previous knowledge with new data in this study permits the investigation of variations in Mg^{2+} that are strictly related to crystallographic changes. This integration is essential to avoid errors in extrapolating information from one organism to another. Contextual high spatial resolution of Mg^{2+} distribution and concentration, coupled with crystallographic information, were obtained using a combination of electron probe microanalysis (EPMA) and electron backscatter diffraction (EBSD) data. EPMA has the advantage over other techniques in determining whether variations in Mg^{2+} are associated with other elements such as sulphur (England *et al.* 2007). In addition, crystallographic data obtained by EBSD match the spatial resolution of EPMA.

1. Material and methods

1.1. Material

The blue mussel *Mytilus edulis* and the rhynchonelliform brachiopod *Terebratulina retusa* were used for this study. Articulated specimens of *T. retusa* were collected at a depth of 200 m in the Firth of Lorn (Oban), NW Scotland, and specimens of *M. edulis* were obtained commercially. 2D sections of shell samples were obtained from cuts along the shell length of ventral and right valves of brachiopod and mussel

 doi:10.1017/S1755691011010036

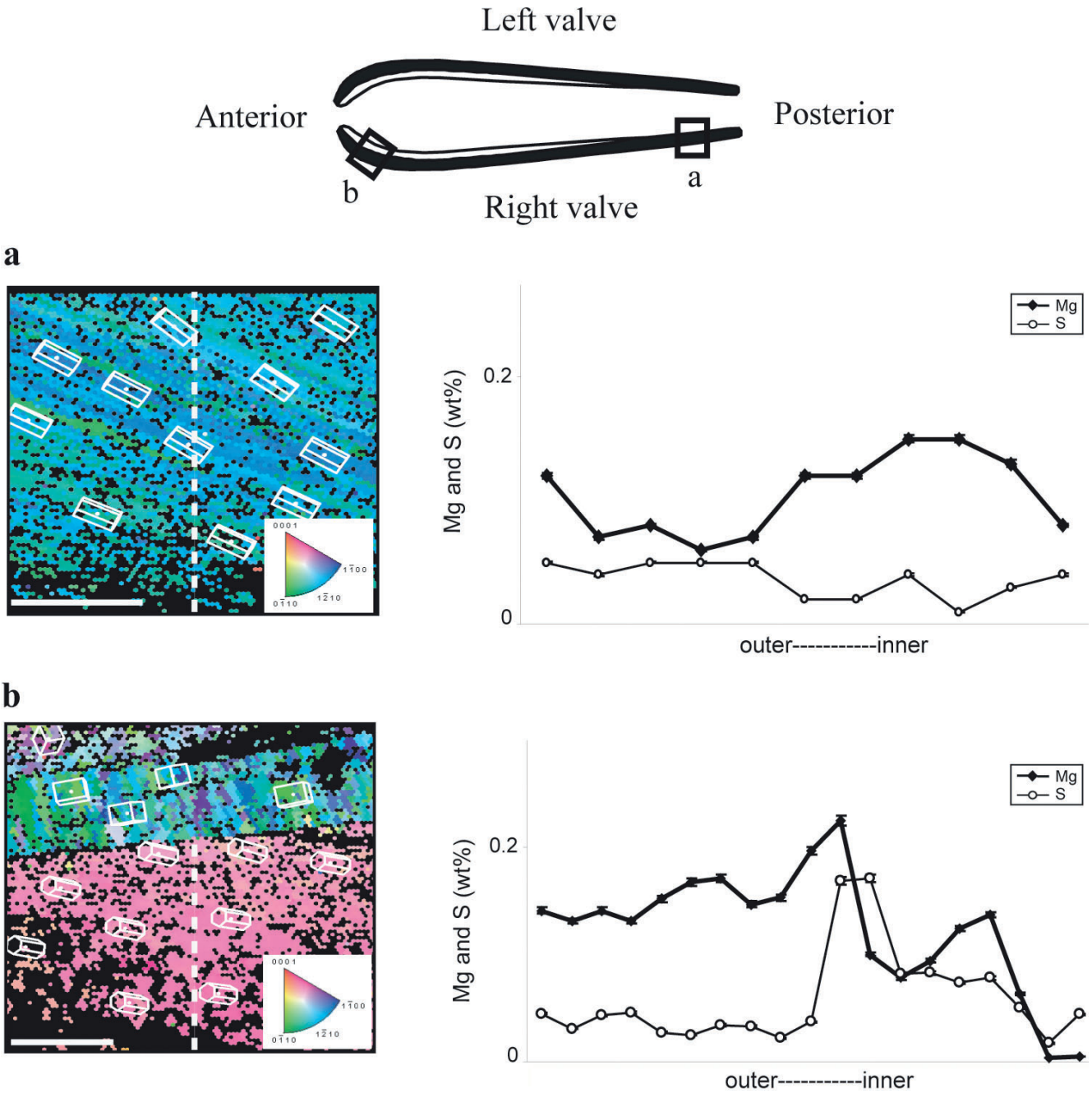

Figure 1 Integrated contextual crystallographic and trace element data at high spatial resolution in posterior (a) and umbo (b) regions of the right valve of *Mytilus edulis*. Left: crystallographic orientation maps across the shell thickness (outer shell surface at the bottom); scale bar in (a)=90 µm, in (b)=60 µm; colours refer to crystallographic planes of calcite (see colour keys); wire frames indicate the orientation of calcite crystals. Right: magnesium and sulphur distribution and concentration across the shell thickness following a transect from the outer to the inner shell surface (indicated by a white dashed line on the crystallographic map); error bars indicate ± 2% relative to internal standards for magnesium and sulphur.

specimens. A similar study was undertaken on equivalent areas of dorsal and left valves (Dalbeck *et al.* 2006; Cusack *et al.* 2007; England *et al.* 2007). Shell sections were mounted in araldite resin blocks, polished and then coated with a thin layer of carbon for EBSD and EPMA analyses.

1.2. Electron backscatter diffraction (EBSD)

Electron backscatter diffraction (EBSD) analyses were performed using a Hikari camera (EDAX) mounted in a FEI Quanta 200F field-emission environmental scanning electron microscope in high (chamber pressure = $5{\cdot}5e^{-6}$ Torr) vacuum mode with an aperture and spot size of 4. The stage is tilted 70° and the electron beam diffracted by interaction of crystal planes in the shell sample. The diffracted beam interacts with a phosphor screen, producing a series of Kikuchi bands that enable crystal identification and orientation to be determined. Data were filtered to remove all data points below a confidence index [CI] of 0·1 and the filtered data analysed using the OIM software from EDAX. Finally, EBSD data were represented by colour-coded crystallographic maps in reference to planes of calcite (further details of technique in Dalbeck *et al.* 2006; Cusack *et al.* 2007; Pérez-Huerta & Cusack 2008).

1.3. Electron probe microanalysis (EPMA)

For EPMA analyses (See Tables 1–3 in Appendix), transects from the outside to the inside of the valves were carried out

https://doi.org/10.1017/S1755691011010036 Published online by Cambridge University Press

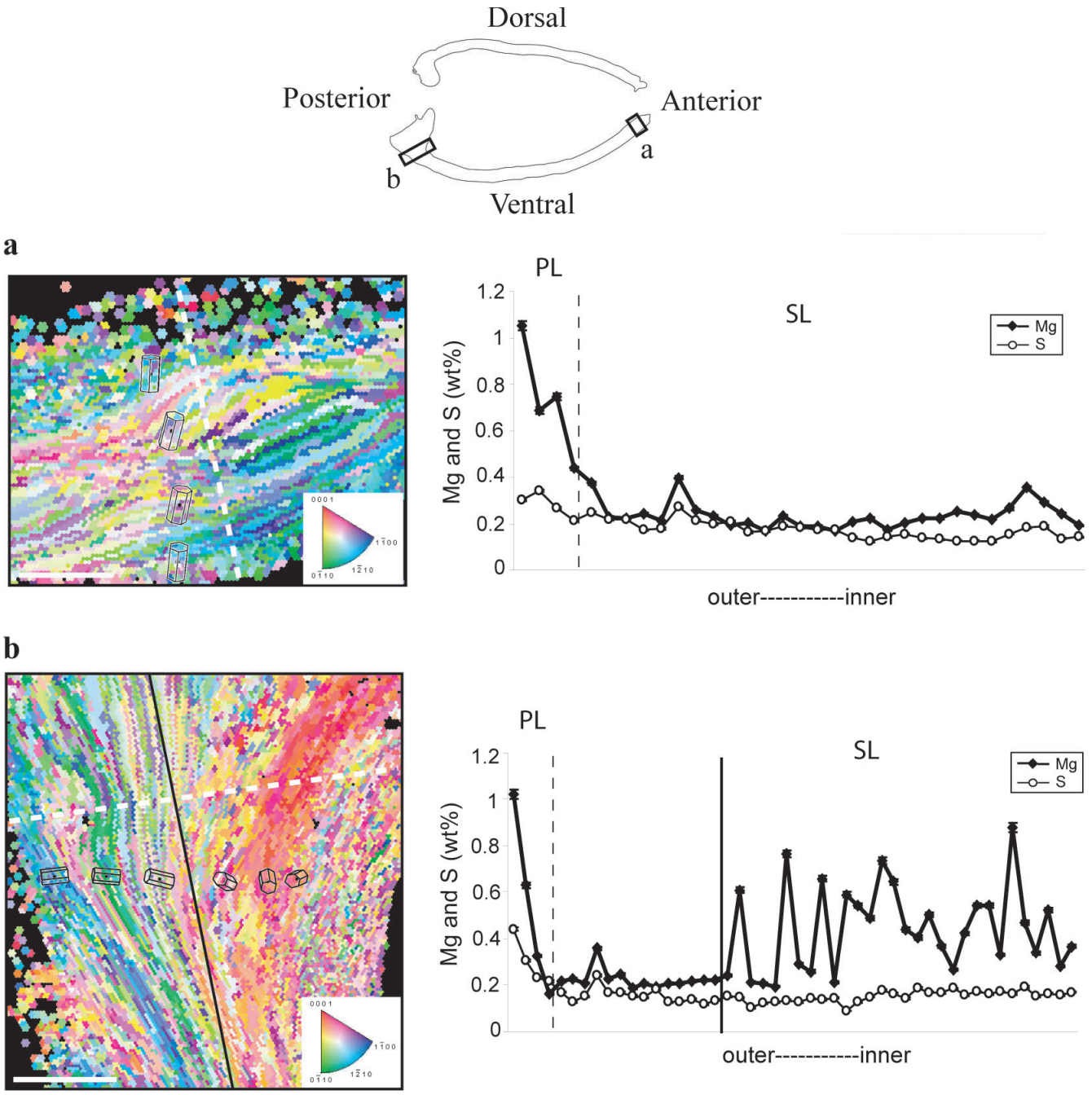

Figure 2 Integrated contextual crystallographic and trace element data at high spatial resolution in anterior (a) and umbo (b) regions of the ventral of *Terebratulina retusa*. Left: crystallographic orientation maps across the shell thickness (outer shell surface at the bottom in (a) and at the left in (b)); scale bar in (a)=200 μm, in (b) =100 μm; colours refer to crystallographic planes of calcite (see colour keys); wire frames indicate the orientation of calcite crystals related to the outer surface. Right: magnesium and sulphur distribution and concentration across the shell thickness following a transect from the outer to the inner shell surface (indicated by a white dashed line on the crystallographic map). Abbreviations: PL=primary layer; SL=secondary layer. Error bars indicate ± 2% relative to internal standards for magnesium and sulphur.

using a Cameca SX50 electron microprobe operating at 15 kV with a 10 nA current and using a 10 μm defocused beam. Matrix corrections used an on-line PAP software correction procedure. The electron microprobe was calibrated using internal mineral standards for Mg (periclase: 60·3% Mg, 39·7% O), S (pyrite: 46·6% Fe, 53·4% S) and Ca (calcite: 40·0% Ca, 12·0% C, 48·0% O). Background counting times were half of the count times on peaks, which were 40 seconds for Mg and S and 30 seconds for Ca. Only analyses above the limit of detection of the SX50 electron microprobe have been considered, with calculated detection limits as follows: Mg (0·027 wt. %) and S (0·033 wt. %). Calculated errors for magnesium and sulphur were ± 2% (mean errors are +/− 2% of the measured number) related to internal standards and standard reproducibility was better than 0·15 SD for both elements. The measured calcium concentrations in our samples vary between 37 and 40 wt. % (see Tables 1–3), which is different from the calcium concentration (39·8 wt. %) used for the development of the equation for Mg/Ca thermometry in *Mytilus edulis* (Vander Putten *et al.* 2000). However, this difference in concentration would not modify significantly the hypothetical calculated temperatures in this study based on a previous study (Pérez-Huerta *et al.* 2008a).

https://doi.org/10.1017/S1755691011010036 Published online by Cambridge University Press

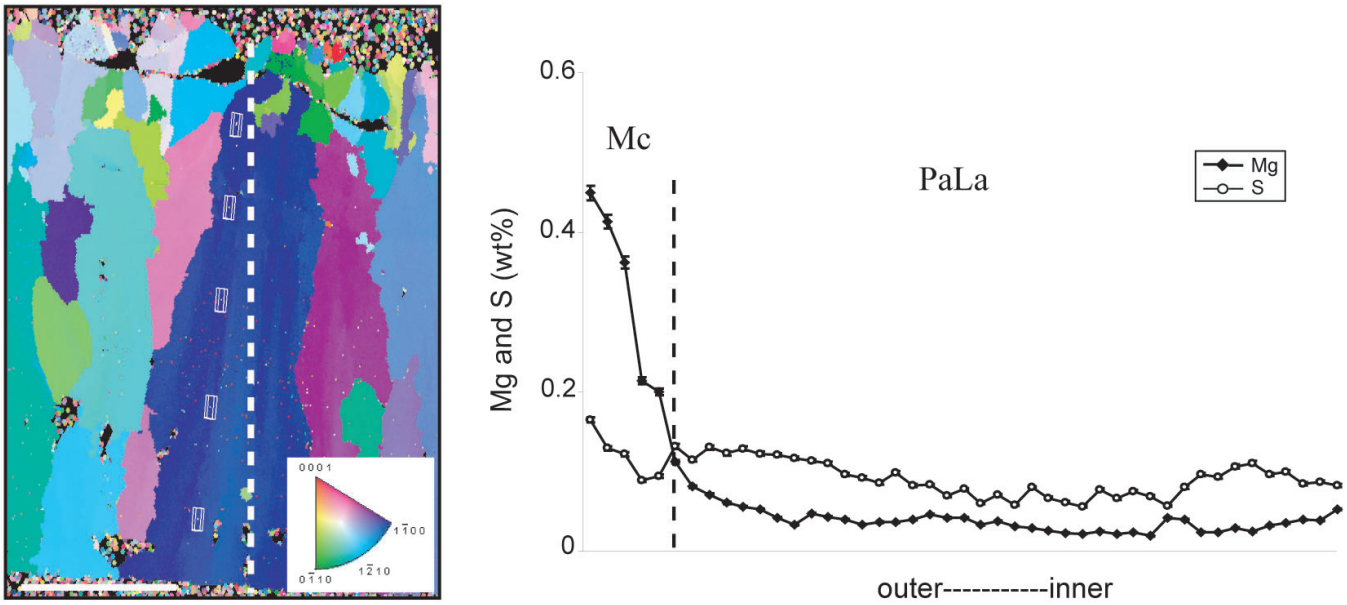

Figure 3 Integrated contextual crystallographic and trace element data at high spatial resolution in the eagle eggshell. Left: crystallographic orientation map across the shell thickness (mamillary caps at the top); scale bar = 100 μm; colours refer to crystallographic planes of calcite (see colour key); wire frames indicate the orientation of calcite crystals, with the *c*-axis normal to the outer surface. Right: magnesium and sulphur distribution and concentration across the shell thickness following a transect from the outer to the inner shell surface (indicated by a white dashed line on the crystallographic map); dark dashed line divides the palisade layer (PaLa) and the mamillary caps (Mc); error bars indicate ± 2% relative to internal standards for magnesium and sulphur.

2. Results

In the umbo and posterior regions of the shell of *Mytilus edulis*, there is crystallographic uniformity across the calcite layer. Therefore, recorded Mg^{2+} variations are not related to crystallographic orientation (Fig. 1). The *c*-axis of calcite crystals rotates 40–65° from the position at the umbo towards the posterior region, with a final orientation at an angle of 30–45° to the outer surface, related to shell growth (Cusack *et al*. 2007). Elemental transects by EPMA throughout show that magnesium concentration varies in the order of 0·1 wt. % across the calcite layer from the outer to inner shell surfaces in the umbo and posterior regions, although the umbo region has a slightly higher concentration (Fig. 1). In contrast, there are compositional variations associated with crystallographic changes in different regions of the shell of *Terebratulina retusa* (Fig. 2). The anterior region is characterised by crystallographic uniformity across the secondary layer, with the *c*-axis of calcite crystals oriented perpendicular to the shell exterior (Fig. 2a). Thus, there are no variations in Mg^{2+} concentration associated with crystallography and the only changes in magnesium (~0·2 wt. %) within the secondary layer correlate with those of sulphur, which has been shown previously for *T. retusa* and other brachiopod species and may be related to the organic matrix (England *et al.* 2007) (Fig. 2). The umbo region presents a different scenario, with changes in crystallographic orientation of calcite crystals and associated major fluctuations in Mg^{2+} concentration (Fig. 2b). The outer part of the secondary layer (~150 μm) is characterised by calcite crystals with *c*-axis perpendicular to the shell surface, but there is a rotation in crystallographic orientation of the *c*-axis of almost 90 degrees towards the inner part (Fig. 2b). The magnesium distribution and concentration in the outer part is similar to that at the anterior region of the shell, but there is sudden increase (~0·5–0·6 wt. %) towards the inner part associated with calcite crystals oriented almost parallel to the shell surface (Fig. 2b). This increase in Mg^{2+} concentration related to the {0001} planes of calcite crystals is in agreement with the sector zoning in abiogenic calcite (Reeder & Grams 1987; Reeder & Paquette 1989) and with the possibility of more substitutions of Ca^{2+} by Mg^{2+} within {0001} crystallographic planes (Reeder 1983). This observation is also in agreement with that of Pérez-Huerta *et al*. (2008b), of magnesium variation using XANES (X-ray absorption near edge structure).

3. Discussion

To establish how Mg^{2+} can vary both with crystallographic planes related to biomineral formation and emplacement, and be independent of variation in seawater temperature, the distribution of magnesium needs to be determined within a scenario of constant ambient temperature and crystallographic uniformity. To address this, a comparison between both bivalved marine invertebrates and avian eggshells was undertaken. Avian eggshells are ideal candidates because they form in a constant temperature environment and the majority of the shell thickness is composed of large calcite crystals with uniform crystallographic orientation (Dalbeck & Cusack 2007). A section across the thickness of an eagle eggshell is used as an example of how much Mg^{2+} concentration may vary within the context of crystallographic uniformity and constant temperature (Fig. 3). The palisade layer, which comprises the majority of the shell thickness, is characterised by large calcite crystals, with the *c*-axis perpendicular to the shell exterior (Dalbeck & Cusack 2007). Magnesium distribution at high spatial resolution reveals that the variation is about 0·1 wt. % across the palisade layer. The scenario described in the eagle eggshell is similar to that of the blue mussel *Mytilus edulis*, in which Mg^{2+} variation is less than 0·2 wt. %, and closer to 0·1 wt. %, within a context of crystallographic uniformity, although *M. edulis* shell formation occurs in a variable temperature environment. These results indicate that there may be at least a variation of about 0·1 wt. % magnesium concentration in calcite biominerals of avian eggshells and

https://doi.org/10.1017/S1755691011010036 Published online by Cambridge University Press

mussels that is not related to either crystallographic or temperature changes.

The results show that variations in Mg^{2+} associated with crystallographic changes can potentially have implications in the application of Mg/Ca thermometry for seawater temperature calculations. In *M. edulis*, there is a variation in Mg^{2+} of 0·1 wt. % that, although not associated with crystallography, could provide misleading seawater estimates (~7°C) based on published equations (e.g. Vander Putten *et al.* 2000). In contrast, Mg/Ca based seawater temperature calculations from *T. retusa* would offer dissimilar results for analyses in different regions of the shell. In umbo regions (Fig. 2b), there is approximately 0·5 wt. % variation in Mg^{2+} associated to crystallography that would theoretically result in seawater temperature miscalculations (>30°C) based on previous studies (e.g. Pérez-Huerta *et al.* 2008a). These results for *M. edulis* and *T. retusa* serve as an example of the importance of including detailed crystallographic data for calcite biominerals in which Mg^{2+} is analysed for Mg/Ca (palaeo)thermometry to avoid errors or misinterpretations by including data unrelated to environmental factors. Thus, the present study confirms earlier claims from several studies in mussels (Vander Putten *et al.* 2000), brachiopods (England *et al.* 2007; Pérez-Huerta *et al.* 2008a) and corals (Meibom *et al.* 2004; Stolarski & Mazur 2005) that some variations in magnesium may be related to crystallography and, therefore, influence environmental interpretations.

4. Concluding remarks

These data suggest that contextual crystallographic information at high spatial resolution should complement Mg^{2+} measurements in calcite biominerals for seawater temperature calculations using Mg/Ca thermometry. The same principle applies to Sr^{2+} and the use of Sr/Ca ratios for temperature calculations, although it is more important in studies with organisms dominated by aragonite biominerals, where the strontium concentration is higher. Results show that changes in crystallographic orientation in calcite crystals, related to biomineral formation and emplacement during shell growth, have a significant effect on magnesium concentrations. The integration of these crystallographic studies and the comparison of two marine bivalved invertebrate organisms with avian eggshells have also revealed that there is commonly approximately 0·1 wt. % variation in Mg^{2+} concentration unrelated to temperature or crystallographic changes. This study demonstrates that the integration of contextual crystallographic, biological and chemical information may be important to extract accurate environmental information from biominerals. In so doing, we will greatly advance our understanding of vital effects, which is of paramount importance for current and future environmental interpretations.

5. Acknowledgements

We would like to acknowledge helpful comments and suggestions by an anonymous reviewer and Dr. Alex Brasier, which have improved considerably the quality of this manuscript, and the help of the Editors and Mrs Vicki M Hammond. AP-H and MC thank the BBSRC (BB/E003265/1) for funding. AP-H (F0719AB) also thanks The Leverhulme Trust and the Department of Geological Sciences (University of Alabama). PD thanks EPSRC (Doctoral Training Award) for financial support. We also thank J. Gilleece, P. Chung, R. McDonald and N. Kamenos for technical advice and support. This work is a contribution to the BioCalc Project of the EuroMinScI Programme (ESF-EUROCORES, ERAS-CT-2003-980409) and Theme 3 (Atmosphere, Oceans and Climate) of SAGES (Scottish Alliance for Geoscience, Environment and Society).

6. Appendix. Tables 1–3

Table 1 EPMA data for *T. retusa*. Totals calculated based on carbonates for $P_2(CO_3)_5$, $S(CO_3)$, $Mg(CO_3)$, $Ca(CO_3)$, $Mn(CO_3)$ and $Sr(CO_3)$, with data only shown in weight (%) for Ca, Mg and S.

T. retusa (Anterior region)				*T. retusa* (Umbo region)			
Ca (wt. %)	Mg (wt. %)	S (wt. %)	Total	Ca (wt. %)	Mg (wt. %)	S (wt. %)	Total
34·77	1·052	0·301	92·8	36·58	1·023	0·440	90·8
36·85	0·687	0·340	96·3	38·13	0·630	0·304	95·4
38·37	0·743	0·267	99·9	38·77	0·325	0·230	97·8
38·42	0·438	0·212	98·9	37·57	0·162	0·216	98·7
38·05	0·373	0·246	97·9	39·91	0·218	0·169	95·7
37·87	0·228	0·218	96·6	38·46	0·226	0·127	101·3
37·15	0·222	0·219	94·9	39·55	0·209	0·151	97·7
38·73	0·242	0·171	98·7	40·18	0·358	0·242	101·5
38·37	0·209	0·177	97·6	38·33	0·228	0·169	102·1
38·79	0·396	0·269	99·8	37·49	0·245	0·168	97·7
37·99	0·256	0·212	96·9	38·50	0·187	0·152	95·2
37·37	0·233	0·197	95·2	40·19	0·207	0·147	97·8
38·37	0·190	0·209	97·7	37·89	0·194	0·182	102·1
37·69	0·200	0·163	96·0	38·38	0·205	0·128	96·2
37·84	0·168	0·169	96·2	38·51	0·205	0·129	97·5
38·17	0·233	0·189	97·4	39·62	0·218	0·140	97·8
39·16	0·188	0·182	99·5	38·81	0·220	0·116	100·6
38·74	0·187	0·171	98·5	37·99	0·222	0·135	98·6
38·21	0·167	0·175	97·1	37·57	0·241	0·152	96·8
38·56	0·209	0·140	98·0	39·57	0·607	0·145	97·0
38·43	0·222	0·121	97·6	39·09	0·211	0·102	100·2
40·12	0·171	0·142	101·8	39·94	0·209	0·122	99·2
39·55	0·204	0·154	100·4	39·01	0·194	0·128	101·2
39·41	0·223	0·137	100·1	39·20	0·765	0·134	101·4
35·66	0·220	0·131	90·7	40·19	0·291	0·128	100·0
37·22	0·250	0·124	94·7	39·14	0·259	0·142	102·1
38·36	0·238	0·124	97·5	37·68	0·658	0·138	101·1
37·76	0·219	0·121	95·9	38·19	0·211	0·144	96·0
37·25	0·264	0·154	95·2	40·21	0·588	0·088	98·1
38·68	0·354	0·180	98·9	37·13	0·543	0·128	103·2
35·81	0·290	0·188	91·6	38·33	0·487	0·150	95·6
39·20	0·240	0·134	99·6	38·59	0·736	0·179	99·5
36·33	0·191	0·141	92·5	39·67	0·645	0·163	99·7
—	—	—	—	40·42	0·438	0·142	101·8
—	—	—	—	36·25	0·405	0·187	103·7
—	—	—	—	39·30	0·503	0·169	93·4
—	—	—	—	40·37	0·369	0·168	100·6
—	—	—	—	39·51	0·267	0·185	103·1
—	—	—	—	38·18	0·422	0·155	101·1
—	—	—	—	37·20	0·541	0·171	98·4
—	—	—	—	39·58	0·542	0·161	95·9
—	—	—	—	38·43	0·330	0·171	101·1
—	—	—	—	39·23	0·879	0·162	100·2
—	—	—	—	40·16	0·469	0·193	101·0
—	—	—	—	39·18	0·339	0·153	102·5
—	—	—	—	34·33	0·523	0·165	100·8
—	—	—	—	38·96	0·279	0·158	87·8

https://doi.org/10.1017/S1755691011010036 Published online by Cambridge University Press

Table 2 EPMA data for *M. edulis*. Totals calculated based on carbonates for $P_2(CO_3)_5$, $S(CO_3)_2$, $Mg(CO_3)$, $Ca(CO_3)$, $Mn(CO_3)$, $Na_2(CO_3)$ and $Sr(CO_3)$, with data only shown in weight (%) for Ca, Mg and S.

M. edulis (Umbo)				*M. edulis* (Posterior)			
Ca (wt. %)	Mg (wt. %)	S (wt. %)	Total	Ca (wt. %)	Mg (wt. %)	S (wt. %)	Total
36·13	0·141	0·045	100·0	39·39	0·120	0·050	100·0
40·26	0·131	0·031	99·9	39·00	0·070	0·040	100·0
39·40	0·141	0·043	100·0	39·25	0·080	0·050	100·0
40·83	0·131	0·046	100·0	39·25	0·060	0·050	100·0
41·14	0·152	0·027	99·9	39·33	0·070	0·050	100·0
40·81	0·168	0·025	100·0	38·72	0·120	0·020	100·0
40·85	0·171	0·034	100·0	39·06	0·120	0·020	100·0
41·00	0·147	0·033	100·0	39·39	0·150	0·040	100·0
40·69	0·153	0·022	100·0	39·32	0·150	0·010	100·0
40·90	0·197	0·037	100·0	38·89	0·130	0·030	100·0
40·60	0·225	0·169	100·0	39·73	0·080	0·040	100·0
40·09	0·100	0·171	100·0	—	—	—	—
41·08	0·078	0·082	100·0	—	—	—	—
40·47	0·094	0·083	100·0	—	—	—	—
41·08	0·124	0·074	100·0	—	—	—	—
40·79	0·137	0·078	99·9	—	—	—	—
38·05	0·063	0·050	99·9	—	—	—	—
38·32	0·003	0·017	100·0	—	—	—	—
37·31	0·005	0·044	99·9	—	—	—	—

Table 3 EPMA data for the golden eagle eggshell. Totals calculated based on carbonates for $P_2(CO_3)_5$, $S(CO_3)_2$, $Mg(CO_3)$, $Ca(CO_3)$, $Mn(CO_3)$, $Na_2(CO_3)$ and $Sr(CO_3)$, with data only shown in weight (%) for Ca, Mg and S.

Golden Eagle Eggshell			
Ca (wt. %)	Mg (wt. %)	S (wt. %)	Total
37·70	0·447	0·149	98·3
38·34	0·412	0·137	99·0
39·11	0·361	0·120	100·2
36·87	0·215	0·071	93·7
39·09	0·201	0·067	99·4
39·46	0·115	0·038	100·2
39·54	0·083	0·028	100·1
39·66	0·074	0·024	100·6
39·51	0·063	0·021	100·1
39·71	0·058	0·019	100·7
39·66	0·056	0·018	100·5
39·07	0·045	0·015	99·0
38·20	0·036	0·012	96·9
39·31	0·050	0·016	99·7
37·17	0·046	0·015	94·5
39·57	0·043	0·014	100·4
39·60	0·037	0·012	100·4
39·79	0·040	0·013	100·7
39·66	0·039	0·013	100·5
39·80	0·043	0·014	100·8
39·54	0·049	0·016	100·1
39·74	0·045	0·015	100·5
39·65	0·045	0·015	100·4
39·83	0·036	0·012	100·9
39·66	0·041	0·013	100·4
39·56	0·034	0·011	99·9
39·45	0·032	0·010	99·8
39·30	0·029	0·009	99·3
39·79	0·026	0·008	100·5
39·99	0·025	0·008	101·0
40·20	0·028	0·009	101·3
39·79	0·024	0·008	100·4
38·65	0·027	0·009	97·5
35·56	0·022	0·007	89·7
36·78	0·045	0·015	92·9
38·51	0·043	0·014	97·5
38·14	0·027	0·009	96·6
37·16	0·027	0·009	94·2
37·29	0·033	0·011	94·5
37·21	0·028	0·009	94·4
37·38	0·036	0·012	94·8
35·97	0·039	0·013	91·3
33·00	0·042	0·014	84·2
33·30	0·042	0·014	85·1
32·33	0·055	0·018	82·3

7. References

Cohen, A. L. & McConnaughey, T. A. 2003. Geochemical perspectives on coral mineralization. *In* Dove, P. M., De Yoreo, J. J. & Weiner, S. (eds) *Biomineralization. Reviews in Mineralogy & Geochemistry* **54**, 151–87.

Cusack, M., Pérez-Huerta, A. & Dalbeck, P. 2007. Common crystallographic control in calcite biomineralization of bivalved shells. *Crystal Engineering Communications* **9**, 1215–18.

Dalbeck, P., England, J., Cusack, M., Lee, M. R. & Fallick, A. E. 2006. Crystallography and chemistry of the calcium carbonate polymorph switch in *M. edulis* shells. *European Journal of Mineralogy* **18**, 601–09.

Dalbeck, P. & Cusack, M. 2007. Crystallography (Electron backscatter diffraction) and chemistry (Electron probe microanalysis) of the avian eggshell. *Crystal Growth & Design* **6**, 2558–62.

England, J., Cusack, M. & Lee, M. R. 2007. Magenseium and sulphur in the calcite shells of two brachiopods, *Terebratulina retusa* and *Novocrania anomala*. *Lethaia* **40**, 2–10.

Erez, J. 2003. The source of ions for biomineralization foraminifera and their implications for paleoceanographic proxies. *In* Dove, P. M., De Yoreo, J. J. & Weiner, S. (eds) *Biomineralization. Reviews in Mineralogy & Geochemistry* **54**, 115–49.

Meibom, A., Cuif, J.-P., Hillion, F., Constantz, B. R., Leclerc, A. J., Dauphin, Y., Watanabe, T. & Dunbar, R. B. 2004. Distribution of magnesium in coral skeletons. *Geophysical Research Letters* **31**, L23306.

Pérez-Huerta, A., Cusack, M., Jeffries, T. & Williams, C. T. 2008a. High resolution distribution of magnesium and strontium and the evaluation of Mg/Ca thermometry in Recent brachiopod shells. *Chemical Geology* **247**, 229–41.

Pérez-Huerta, A., Cusack, M., Janousch, M. & Finch, A. 2008b. Influence of crystallographic orientation of biogenic calcite on *in situ* Mg XANES analyses. *Journal of Synchrotron Radiation* **15**, 272–75.

Pérez-Huerta, A. & Cusack, M. 2008. Common crystal nucleation mechanism in shell formation of two morphologically distinct calcite brachiopods. *Zoology* **111**, 9–15.

Reeder, R. J. 1983. Crystal chemistry of rhombohedral carbonates. *In* Reeder, R. J. (ed.) *Carbonates: Mineralogy and Chemistry. Reviews in Mineralogy* **11**, 1–47.

Reeder, R. J. & Grams, J. C. 1987. Sector zoning in calcite cement crystals – Implications for trace element distribution in carbonates. *Geochimica et Cosmochimica Acta* **51**, 187–94.

Reeder, R. J. & Paquette, J. 1989. Sector zoning in natural and synthetic calcites. *Sedimentary Geology* **65**, 239–47.

Stolarski, J. & Mazur, M. 2005. Nanostructure of biogenic versus abiogenic calcium carbonate crystals. *Acta Palaeontologica Polonica* **50**, 847–65.

Urey, H. C., Lowenstam, H. A., Epstein, S. & McKinney, C. R. 1951. Measurement of paleotemperatures and temperatures of the Upper Cretaceous of England, Denmark and the southeastern United States. *Geological Society of America Bulletin* **62**, 399–416.

Vander Putten, E., Dehairs, F., Keppens, E. & Baeyens, W. 2000. High resolution distribution of trace elements in the calcite shell layer of modern *Mytilus edulis*: environmental and biological controls. *Geochimica et Cosmochimica Acta* **64**, 997–1011.

https://doi.org/10.1017/S1755691011010036 Published online by Cambridge University Press

Weiner, S. & Dove, P. M. 2003. An overview of biomineralization processes and the problem of the vital effect. *In* Dove, P. M., De Yoreo, J. J. & Weiner, S. (eds) *Biomineralisation. Reviews in Mineralogy & Geochemistry* **54**, 1–29.

MS received 23 February 2010. Accepted for publication 28 October 2010.